JOURNAL OF AIRCRAFT
Vol. 43, No. 6, November–December 2006

Vortex Behaviors of Rolled Supersonic Transport Configuration with Leading-Edge Flaps

Kenichi Rinoie* and Masashi Shirotake†
University of Tokyo, Tokyo 113-8656, Japan
and
Dong Youn Kwak‡
Japan Aerospace Exploration Agency, Tokyo 181-0015, Japan

DOI: 10.2514/1.21470

Wind tunnel measurements were done to investigate the effect of leading-edge flaps on the rolling moment characteristics of the cranked arrow wing for the supersonic transport. Static rolling moment measurements, flow visualization studies, and crossflow velocity measurements by a particle image velocimetry were made at $Re = 6.2 \times 10^4$. Static rolling moment measurements confirmed linear restoring moment at $\alpha < 16$ deg for the models both with and without flap deflection. When the outboard leading-edge flap is deflected 12 deg, rolling moment hysteresis is observed at the roll angle of $\phi \approx 20$ deg and $\alpha \approx 20$ deg. The experimental results indicate that the hysteresis is caused by different vortex breakdown behaviors on the inboard wing when the wing is rotated in the clockwise and counterclockwise directions.

Nomenclature

$b_{\max}$	=	wing maximum span length, m
$\bar{c}$	=	wing mean aerodynamic chord, m
c_r	=	wing root chord at model centerline, m
C_{roll}	=	rolling moment coefficient nondimensionalized using $b_{\max}$ measured about body axis x
L/D	=	lift/drag ratio
Re	=	Reynolds number based on mean aerodynamic chord
U_∞	=	freestream velocity, m/s
V	=	mean velocity in y direction, m/s
w	=	mean velocity in z direction, m/s
w_b	=	mean velocity in z_b direction, m/s
x	=	chordwise coordinate measured from apex of delta wing at model centerline, m
y	=	horizontal coordinate orthogonal to x, measured from model centerline, m
y_b	=	spanwise coordinate orthogonal to x, fixed to the body and measured from model centerline, m
z	=	coordinate orthogonal to x and y measured from model centerline, m
z_b	=	coordinate orthogonal to x and y_b measured from model centerline, m
α	=	wing angle of attack, degree
δ_{fLE}	=	outboard leading-edge flap deflection angle, degree
ϕ	=	roll angle, degree (clockwise direction is positive when seen from downstream of the model)
θ	=	incidence angle, degree
ξ	=	vorticity in y-z plane, see Eq. (1)

Presented as Paper 2004-4.1.3 at the 24th International Council of the Aeronautical Sciences Congress (ICAS), Yokohama, Japan, 29 Aug.–3 Sep. 2004. Received 29 November 2005; revision received 16 February 2006; accepted for publication 21 February 2006.

*Professor, Department of Aeronautics and Astronautics, 7-3-1 Hongo, Bunkyo-ku. Senior Member AIAA.
†Graduate Student, Department of Aeronautics and Astronautics, 7-3-1 Hongo, Bunkyo-ku.
‡Senior Researcher, Aviation Program Group, 6-13-1 Osawa, Mitaka. Member AIAA.

I. Introduction

A delta wing planform is often used for high speed aircraft such as a supersonic transport (SST) because of its good supersonic performance. Since the aspect ratio of the delta wing is relatively small, the lift curve slope of the delta wing is also low and the delta wing aircraft has to fly at a high angle of attack at the low speeds of takeoff and landing. At high angles of attack a pair of leading-edge vortices is formed on the delta wing producing suction lift, associated with a high drag.

At high angles of attack, the delta wing will sometimes experience a self-induced roll oscillation known as wing rock [1]. The wing rock originates from the dynamically unstable rolling moment generated by the leading-edge vortices. When the delta wing is rolled, the effective sweepback angles on the windward and leeward wings are different [1]. This asymmetry induces the asymmetric formation of the leading-edge vortices and the wing exhibits complex aerodynamic behaviors. Therefore, static rolling moment characteristics are one of the important factors for the aerodynamic design of delta wing aircraft.

In the case of the main wing of the supersonic transport configuration, it has either a double delta wing or a cranked arrow wing, both having different leading-edge sweepback angles at the inboard and outboard leading edges. Two pairs of leading-edge vortices are formed on the inboard and outboard wings. These vortices interact with each other, making wing characteristics different from those of a plain delta wing [2,3]. These complex static roll characteristics of these wings will be studied here. As far as the authors know, there are only a few references on the static roll characteristics of either the double delta wing or the cranked arrow wing [4].

The lift/drag ratio at low speeds is an essential factor for the improvement of the take-off and climb performance of the SST. The L/D of the delta wing aircraft is relatively poor, because of the high drag as mentioned above. To improve the lift/drag ratio of the SST, a leading-edge device such as a vortex flap or a leading-edge flap can be used. The vortex flap utilizes the suction force generated by the vortex formed on the deflected flap surface with its highly swept leading-edge reducing the drag and improving the lift/drag ratio of the wing [5,6].

As for the SST configuration, the vortex flap and the leading-edge flap can be used for the inboard wing and the outboard wing, respectively, because the inboard wing has a higher sweepback angle and the outboard wing a lower sweepback angle. Therefore, in [7], the authors applied the leading-edge vortex flaps and the leading-

edge flaps on the cranked arrow wing SST configurations. Results indicated that the combination of the leading-edge vortex flaps on the inboard wing and the leading-edge flaps on the outboard wing provides a high lift/drag ratio benefit in a wide lift coefficient range.

It is of interest to see how the deflection of leading-edge flaps affects the rolling moment characteristics of the cranked arrow SST wing. Static rolling moment measurements for the SST with vortex flaps and leading-edge flaps have been carried out in [8]. Results indicated that a nonlinear and abrupt change of the rolling moments occurred when the flaps were deflected. However, details of the vortex behavior affecting the rolling moment characteristics were not obtained. Therefore, experimental studies using a particle image velocimetry (PIV) were made to reveal this complex vortex behavior causing the nonlinear and abrupt change of static rolling moments for the SST model with leading-edge flaps.

The SST configuration used in this study is of a smaller scale but similar in planform configuration to that used in [7–9]. It is based on the cranked arrow wing configuration that was designed for the supersonic flight test program, which is currently underway at the Japan Aerospace Exploration Agency. The leading-edge of this wing was modified so that it has vortex flaps for the inboard section and leading-edge flaps for the outboard section. However, results indicated that the effect of the inboard vortex flap deflection on the roll characteristics was very small compared with that of the outboard leading-edge flap deflection. Hence, only the results of outboard leading-edge flap deflection are shown and discussed in this paper.

Experiments were conducted in a 0.6×0.6 m blowdown low-speed wind tunnel. The Reynolds number based on the mean aerodynamic chord was 6.2×10^4. PIV measurements were conducted to investigate the flap deflection effects on the static rolling moment characteristics in detail.

In summary, the purpose of this study is to discuss the effect of leading-edge flap deflections on the static roll characteristics of the cranked arrow SST configuration and to clarify the complex behavior of the leading-edge separation vortices formed on the wing.

II. Experimental Conditions

Figure 1 shows the model details. This SST configuration model is based on the cranked arrow wing configuration with a fuselage section that was preliminarily designed for the supersonic flight test program conducted by the Japan Aerospace Exploration Agency [10]. The present wind tunnel model is 1/5 scale of the original wind tunnel model. Although the original model, used in [7–9], had a warped wing section, the current model wing is a flat plate of 0.001 m thickness. The upper and lower surfaces are all beveled. The wing has an inboard sweepback angle of 66 deg and 42 deg at the outboard section. The kink is located between the inboard and outboard wings at $y/(b_{\max}/2) = 0.55$ and this model was modified so that it has the leading-edge flaps on the outboard wing (Fig. 1). The chord of the outboard leading-edge flap is 20% of the local chord at each spanwise station. The leading-edge flap deflection angle δ_{fLE} for the outboard wing is defined as the angle measured parallel to the freestream. The tested flap deflection angles are $\delta_{\mathrm{fLE}} = 0$ and 12 deg. The nose section, that is 25% of the total fuselage length, is an ogive-cone cylinder.

The experiments were made in a 0.6×0.6 m blowdown type low-speed wind tunnel at the University of Tokyo. Tests were made at a tunnel speed of $U_\infty = 10$ m/s. The Reynolds number based on the mean aerodynamic chord ($\bar{c} = 0.087$ m) was $Re = 6.2 \times 10^4$. The incidence angle θ was in a range from 0 to +30 deg. (This angle is equal to the angle of attack at the roll angle $\phi = 0$ deg.) Rolling moment was measured using a two-component balance. This balance has two elements in parallel and is made of aluminum. The sum of the outputs from these two elements gives normal force and the difference of the two gives rolling moment. The model was attached to the balance with a sting and could with balance be rotated around its center axis with balance using a stepping motor. The rolling moment is the roll component around the model center axis (Fig. 2). The rolling moment coefficient has been obtained by rolling the model at 2 deg increments from $\phi = -30$ to +30 deg and back from $\phi = +30$ to -30 deg, all in one cycle of the measurements. The model was at rest at each prescribed roll angle ϕ for about 3.5 s, while

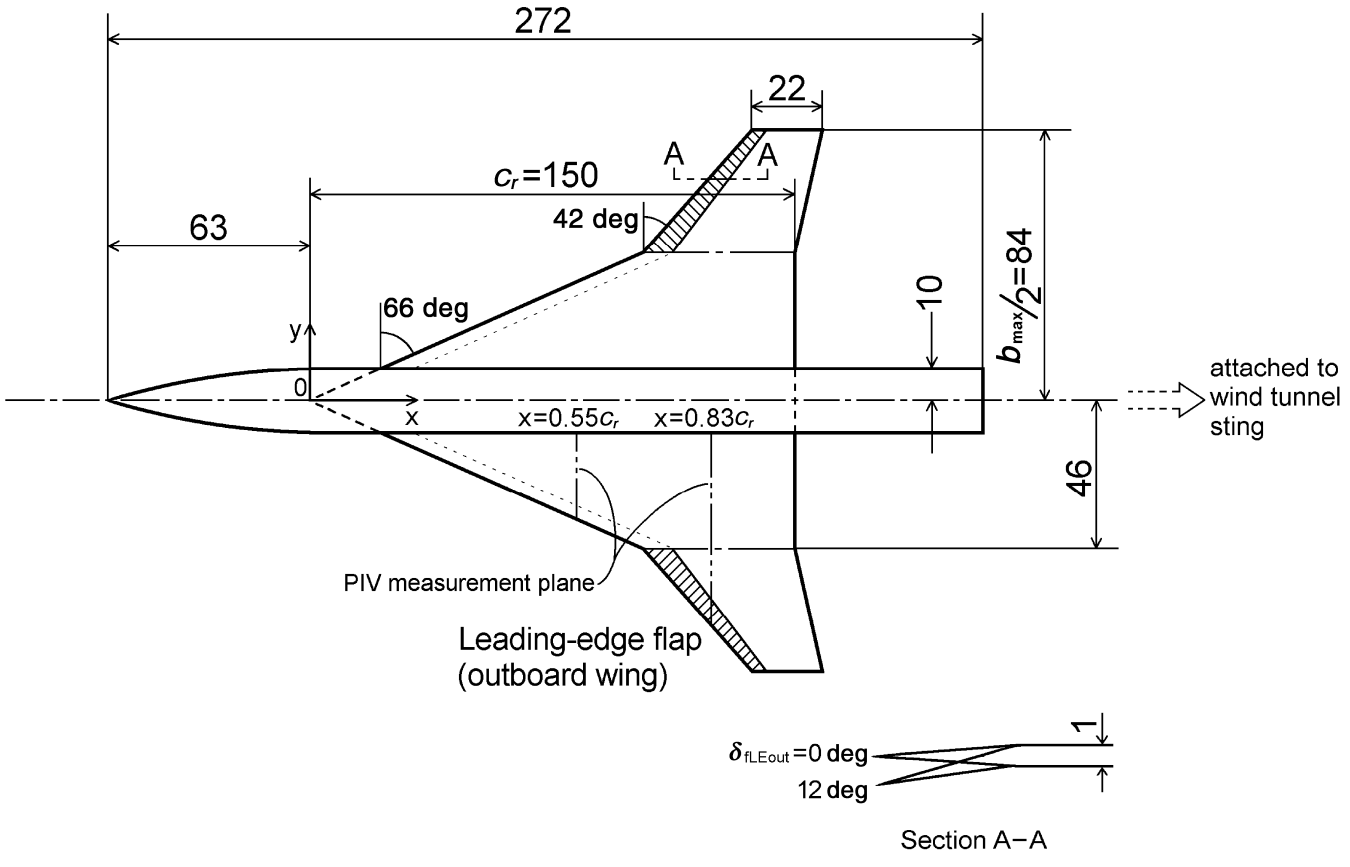

Fig. 1 SST model, in millimeters.

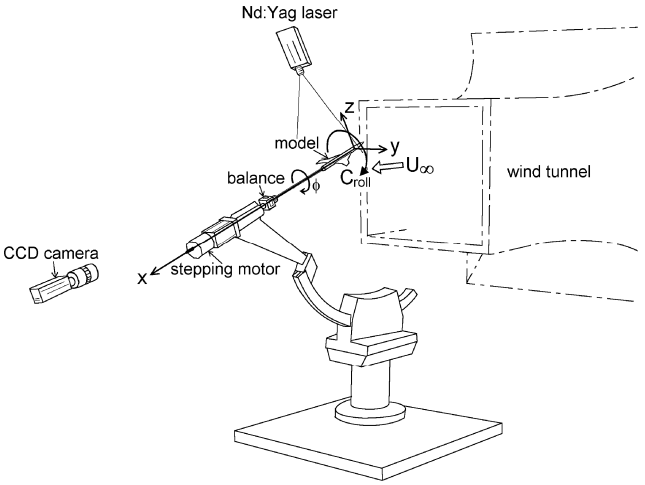

Fig. 2 Experimental setup.

the rolling moment measurements were conducted. This measurement was repeated for 10 cycles and the mean value of C_{roll} was obtained. The definition of C_{roll} and the x, y, z coordinate system used are indicated in Fig. 2. Please note that the x, y, z systems are dependent on the model incidence angle but independent of the model roll angle. All of the aerodynamic coefficients were calculated based on the original wing area without any flap deflection. The estimated overall uncertainty of the aerodynamic coefficients is at most $\pm 2\%$.

Examples of the notation used in this paper are as follows. S00 is the original wing without flap deflection and S12 is the wing with $\delta_{\text{fLE}} = 12$ deg. In [7], S00 is S000000 and S12 is S001200. In this paper the notation was changed for simplicity.

The PIV system used here was the Dantec PIV 2000 Flowmap system with 50 mJ dual cavity Nd:Yag lasers. Mist made of ondina oil (a water white oil blended from mineral oil) was used to seed the wind tunnel. The two-dimensional velocity distributions v, w in the y-z plane normal to the model center axis x were measured at different chordwise stations. PIV measurements were repeated for two planes within the flow field over the left wing at the chordwise station $x = 0.83c_r$. The typical measurement plane of 0.04×0.04 m^2 resulted in 62×62 velocity vectors. The flow over the right wing at the roll angle of ϕ was assumed to be the same as that for the left wing at the roll angle of $-\phi$. Measurements were repeated 300 times at each plane with a velocity acquisition rate of 7.5 Hz. Intervals between laser pulses were set to be 25 μs. The standard data validation method [11] was used in obtaining mean velocities as ensemble averages with an uncertainty of $\pm 6\%$ of U_∞ using the error estimation method of [12]. The laser light sheet used for the PIV measurements was set normal to the model surface. Vorticity ξ has been estimated using the measured velocity data v, w. ξ is defined by

$$\xi(m,n) = \{w(m+1,n) - w(m-1,n)\}/\Delta y - \{v(m,n+1) - v(m,n-1)\}/\Delta z \quad (1)$$

where $\xi(m,n)$ is the vorticity at grid position m, n, and Δy, Δz are the grid spacing in the y and z directions (velocity data are given on a discrete grid in the PIV measurement plane). ξ is nondimensionalized by U_∞ and $\bar{c}$. The vorticity ξ is the only component of the vorticity that can be measured by use of the present two-dimensional PIV system. The vorticity considered here is the most intense component in the vortices, because the PIV system measures their swirl strength.

Since some CCD sensor pixels of the CCD camera used for the PIV measurements (light sensitive pixel number of the CCD camera: 1008×1018) had been damaged accidentally, the correct velocity distributions could not be obtained around these sensor pixel areas (in the ovals in the PIV results, for example, see Sec. III). When the wing roll angle is increased, the rear part of the model disturbed the visibility of the CCD camera. Therefore, the PIV measurements at the left side of the tip region of the left wing could not be conducted correctly when $\phi > 0$ deg. This disturbed area is indicated in the oval.

When the PIV measurements and the balance measurements were conducted at the same time (III.B.2), the velocity acquisition by the PIV was made to obtain five pictures at each roll angle ϕ. By repeating the roll cycle ($\phi = -30 \rightarrow +30 \rightarrow -30$ deg) 60 times, 300 pictures were obtained for each ϕ, good averaged velocity distributions were obtained.

Smoke flow visualization was used to describe the flow around the model, using the oil mist used for the PIV measurements. The light sheet used to illuminate the flow was normal to the x axis. The smoke visualization picture was taken from downstream of the model. Smoke visualization tests were conducted at $U_\infty = 10$ m/s. These visualization tests were made separately from force and PIV measurements and one of the typically observed smoke patterns is shown in each figure in this paper.

Although it is often discussed that the formation of the leading-edge vortices on the delta wing weakly depends on the Reynolds number, the present experiments were conducted at low Reynolds number. The effect of the Reynolds number is discussed in Sec. III.B.

III. Results and Discussion

A. Original Wing Without Flap Deflection

In this section, the performance of the original wing without flap deflection (S00) is summarized and discussed. Figure 3 shows the results of static rolling moment characteristics C_{roll} versus roll angle ϕ for different incidence angles θ without flap deflection (S00). This figure shows that a linear restoring (stable) rolling moment is acting at the incidence angles θ of 12 and 14 deg. As explained in [13], at relatively low incidence angles, the increase in the effective sweepback angle on the leeward wing and decrease on the windward wing produce the restoring rolling moment. As the incidence angle is increased, the linearity observed at lower θ is gradually lost. At $\theta = 26$ deg, C_{roll} indicates that restoring and unstable rolling moment distributions alternate. At $\theta = 28$ deg, C_{roll} drastically changes its state from stable to unstable. This is also observed at $\theta = 30$ deg.

Figure 4 shows the cross flow velocity and vorticity distributions over the wing measured at 83% root chord ($x = 0.83c_r$) by the PIV for the S00 configuration at $\theta = 20$ deg and $\phi = 0$, 10, and 20 deg. Smoke flow pictures taken of the same configurations are also

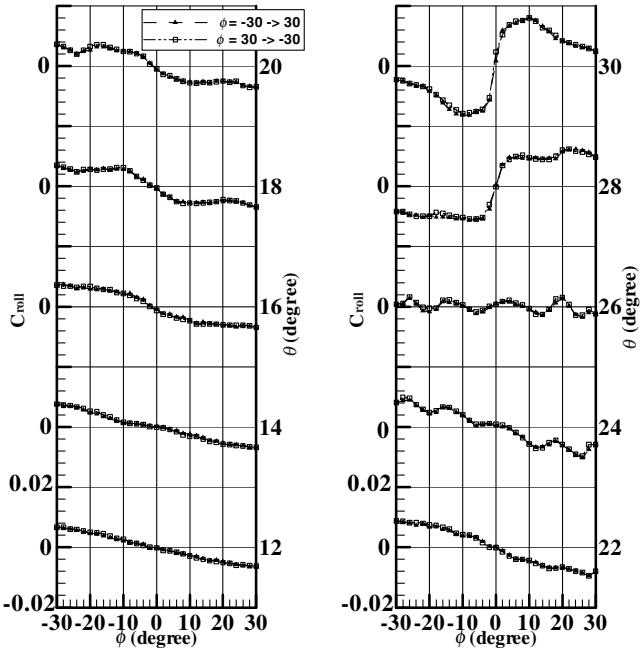

a) $\theta = 12-20$ deg b) $\theta = 22-30$ deg

Fig. 3 Rolling moment characteristics at different incidence angles, S00 (without flap deflection).

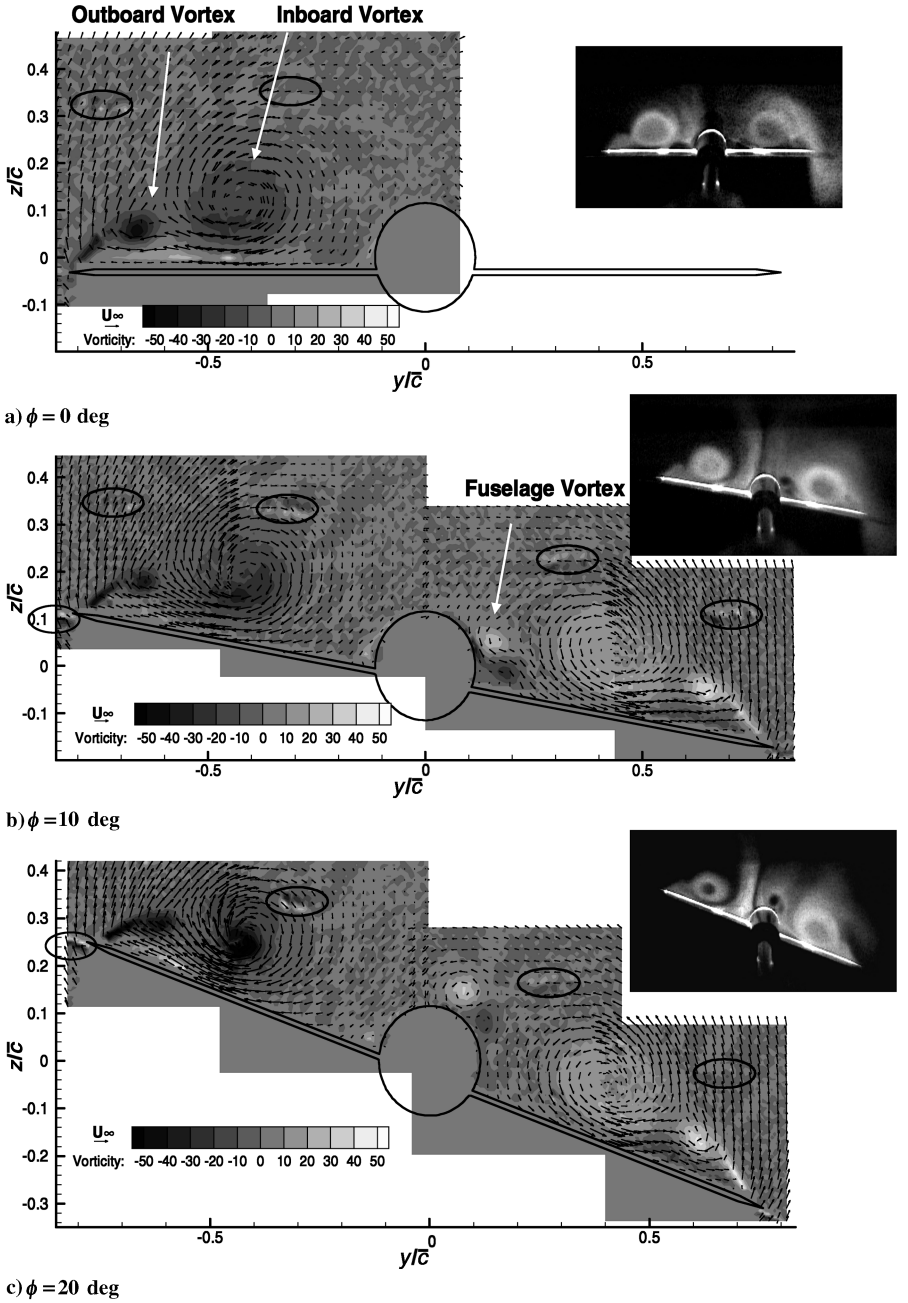

a) $\phi = 0$ deg

b) $\phi = 10$ deg

c) $\phi = 20$ deg

Fig. 4 Crossflow velocity and vorticity distributions of S00 (without flap deflection) together with smoke flow pictures at $\theta = 20\,\text{deg}$, $x/c_r = 0.83$.

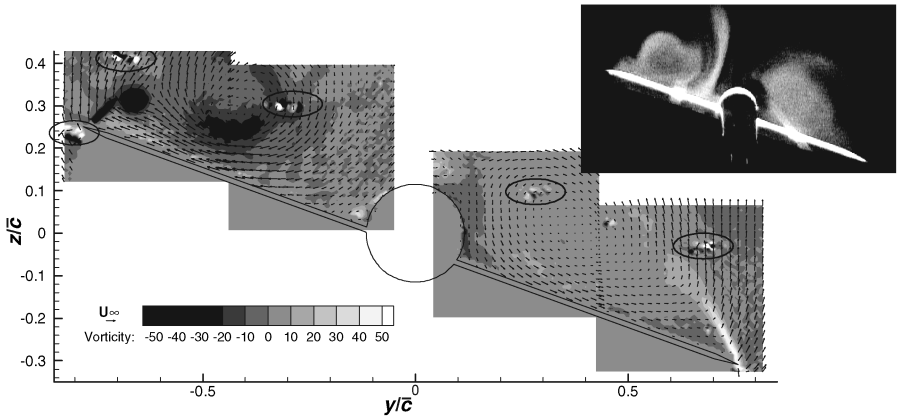

Fig. 5 Crossflow velocity and vorticity distributions of S00 (without flap deflection) together with smoke flow pictures at $\theta = 26\,\text{deg}$, $\phi = 20\,\text{deg}$, and $x/c_r = 0.83$.

shown. In this paper the number of velocity vectors in each PIV measuring plane has been reduced to 21×21 vectors for easiness in viewing the results. At $\phi = 0$ deg (Fig. 4a, left wing only), the formations of inboard vortex ($y/\bar{c} = -0.4$) and outboard vortex ($y/\bar{c} = -0.7$) are clearly visible. The outboard vortex originates from the kink of the cranked arrow wing. As the wing is rolled to $\phi = 10$ and 20 deg, the absolute value of the vorticity ξ increases at the center region of the inboard vortex on the leeward wing (left wing). A smoke-free region is clearly visible near the vortex core in the picture when $\phi = 20$ deg. The high amount of vorticity and the smoke-free region are due to a large tangential velocity existing upstream of the vortex breakdown. In this paper, vortex breakdown will be mainly identified both from the vorticity distributions and from the smoke visualization pictures. The wing roll increases the effective sweepback angle of the leeward wing, causing the vortex breakdown to move toward the trailing edge, creating stronger vortices upstream of the breakdown point [14]. The vortex formed along the fuselage is also observed in Fig. 4. As the roll angle is increased, this vortex apparently moves from the right side of the fuselage (Fig. 4b) to the top of the fuselage (Fig. 4c).

Figure 5 shows flow visualization results for the S00 configuration at $\theta = 26$ deg and at $x = 0.83c_r$ when $\phi = 20$ deg. The vorticity of the inboard vortex on the leeward wing is much smaller than that at $\phi = 20$ deg (Fig. 4c) and the picture in Fig. 5 indicates no clear smoke-free region near the vortex core. This indicates that breakdown of the leading-edge vortices have occurred on this configuration. The outboard vortices on the windward and leeward wings are located much farther away from the wing surface than at $\theta = 20$ deg.

Kwak et al. [9] investigated the rolling moment characteristics of the rolled SST configuration without flap deflection, with a similar plane shape to that of the present model as was described in section II. The Reynolds number of [9] was $Re = 9.2 \times 10^5$, much higher than in the present case. Results in [9] indicated that a linear stable rolling moment was observed at low incidence angles, as in Fig. 3, but that a change from stable to unstable rolling moments was observed at $\theta = 20$ deg. This switching incidence angle is lower than that of the present experiments. Kwak et al. [9] showed how the switch from stable to unstable characteristics could have been caused by the asymmetric movement of the chordwise location on the vortex breakdown on windward and leeward wings. Although the switching incidence angle is different for the present results, the abrupt changes of the rolling moment at higher incidence angles in this study are thought to be attributable to asymmetric vortex breakdown.

B. Wing with Outboard Flap Deflection

Figure 6 shows C_{roll} (ϕ) for different θ with the outboard flap deflection $\delta = 12$ deg (S12). This figure indicates a linear restoring rolling moment until $\theta > 16$ deg. Nonlinear rolling moment characteristics are seen at $\theta \geq 18$ deg. Both restoring and unstable rolling moment distributions are observed alternately at $\theta = 28$ deg. Unstable static roll characteristic are observed for all the measured roll angles at $\theta = 30$ deg. Furthermore, at $\theta = 20$ deg, rolling moment hysteresis is observed at the roll angle axis between $\phi = \pm 20$ and ± 22 deg (i.e., different rolling moment is measured when the model is rolled in the clockwise (from $\phi = -30$ to $+30$ deg) and the counterclockwise direction (from $\phi = -30$ to $+30$ deg). Similar static rolling moment hysteresis has been observed for 65 and 80 deg delta wings [15,16].

Figure 7 shows the crossflow velocity and vorticity distributions over the wing at $x = 0.83c_r$ for the S12 configuration at $\theta = 20$ deg together with the smoke visualization pictures. When the results at $\phi = 0$ deg (Fig. 7a) are compared with the results for S00 (Fig. 4a), it can be seen that the deflection of the outboard wing has little effect on the formation and location of the inboard primary vortex. However, the outboard vortex (at $y/\bar{c} = -0.7$) is located much closer to the surface and farther away from the inboard vortex than in the case of S00 because of the outboard flap deflection. Figure 7b shows that at $\phi = 10$ deg the outboard vortices formed on both windward and leeward wings are still located closer to the surface than for S00 at the same condition (Fig. 4b). Furthermore, the absolute values of the vorticity at the center of the outboard vortices are slightly higher for S12 than for S00. Figure 7c shows results for S12 at $\phi = 20$ deg that are very similar to those observed at $\phi = 10$ deg.

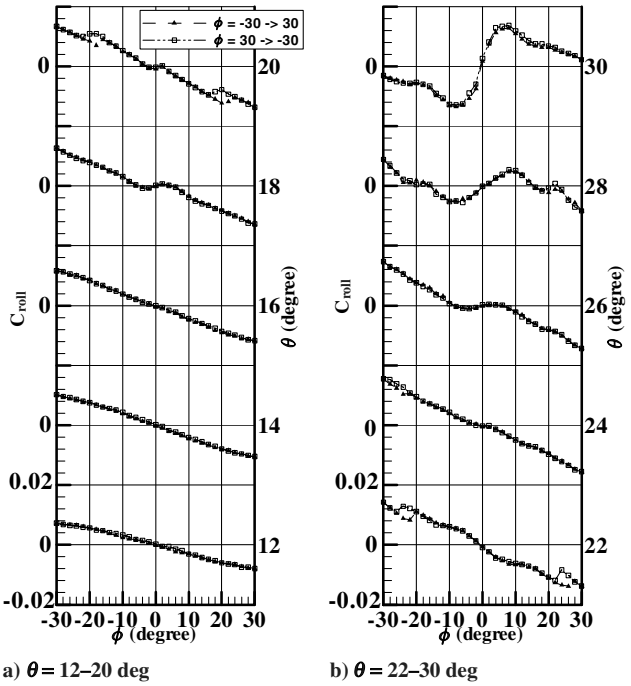

Fig. 6 Rolling moment characteristics at different incidence angles, S12 (with outboard flap deflection $\delta_{\text{fLE}} = 12$ deg).

1. *Rolling Moment Hysteresis Measurements*

The rolling moment hysteresis cannot be determined from Fig. 7c, because each PIV measurement at different roll angles was done independently. It has been thought that the PIV measurements should be conducted in a manner similar to those for the rolling moment described in Experimental Conditions. Figures 8 and 9 show the crossflow velocity and vorticity distributions over the wing for the S12 configuration at $\theta = 20$ deg and at $x = 0.83c_r$ together with smoke visualization pictures, and PIV measurements conducted as described above. Figure 8 shows the results at $\phi = 18$, 20, 22, and 24 deg when the model is rolled in the clockwise direction as seen from downstream of the model. Figure 9 shows the corresponding results when the model is rolled in the counterclockwise direction. It should be noted that the measurements were done from $\phi = -30$ to $+30$ deg in Fig. 8 and from $\phi = +30$ to -30 deg in Fig. 9 thereby conducting the measurements at the same flow condition as for the rolling moment measurements.

Figures 8a and 9a indicate that there are almost no differences between the PIV results for clockwise and counterclockwise rotation at $\phi = 18$ deg. Figures 8d and 9d show similar indifference at $\phi = 24$ deg. However, at $\phi = 20$ deg and 22 deg, differences are observed in the inboard vortex on the leeward (left) wing between the results for clockwise and counterclockwise rotation, the set of Figs. 8b and 9b versus the set of Figs. 8c and 9c. When the model is rolled in the counterclockwise direction (Figs. 9b and 9c), the inboard vortex core on the leeward wing is clearly distinguished in the velocity distributions (by its high vorticity at the center of the vortex), as well as in the smoke pictures. On the other hand, according to the results in the clockwise direction (Figs. 8b and 8c), the center of the inboard vortex on the leeward wing is not clearly visible and the absolute value of vorticity at the outboard vortex is lower than in Figs. 9b and 9c. As for the windward wing (right wing), the inboard vortices in all the figures show very similar distributions. This means that the static flow conditions are not affected by the rolling direction on the windward wing at $\phi = 20$ deg and $\phi = 22$ deg.

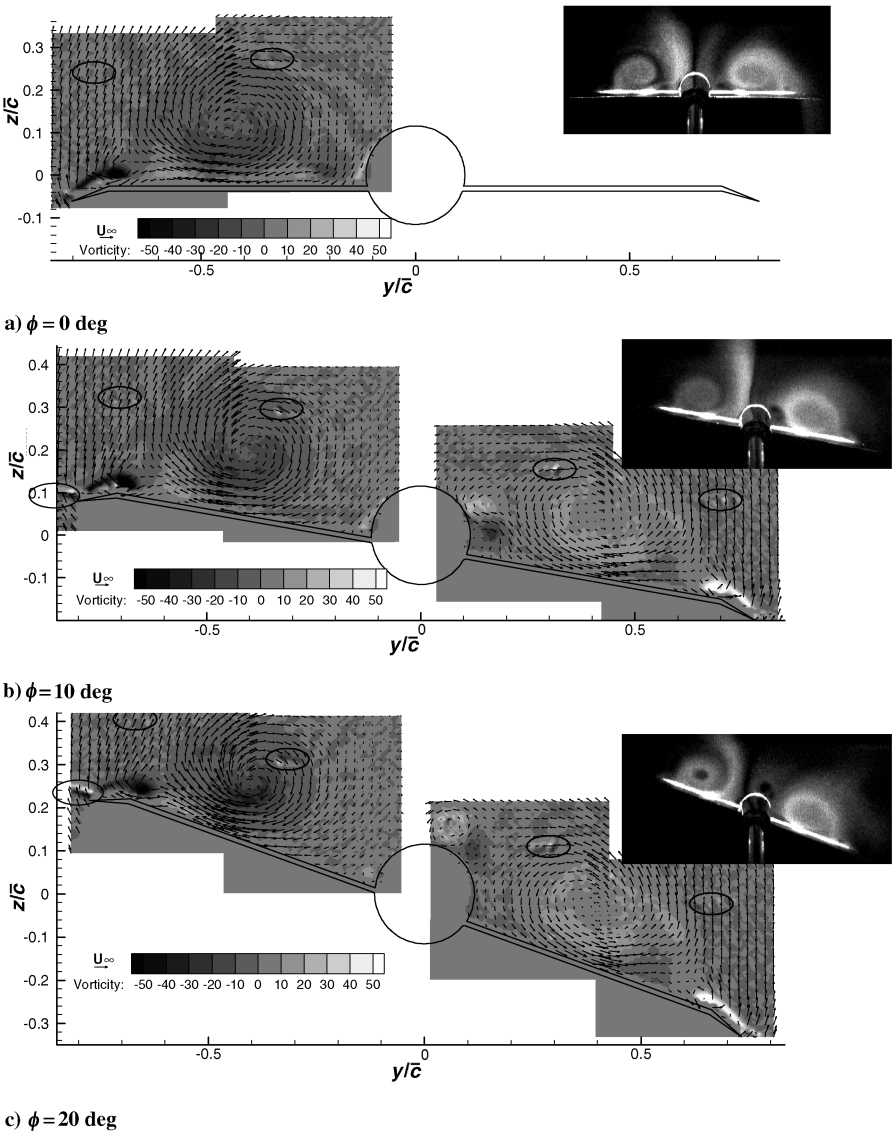

Fig. 7 Crossflow velocity and vorticity distributions of S12 (with outboard flap deflection $\delta_{\mathrm{fLE}} = 12\,\mathrm{deg}$) together with smoke flow pictures at $\theta = 20\,\mathrm{deg}$, $x/c_r = 0.83$.

From the results in Figs. 8 and 9 it can be concluded that the inboard vortex on the leeward wing tends to keep its vorticity at the core high. As a result the vortex does not break down until at much lower roll angle when the model is rolled in the counterclockwise direction (Figs. 9b and 9c) than when the model is rolled in the clockwise direction (Figs. 8b and 8c), causing the chordwise position of the vortex breakdown of the inboard vortex on the leeward wing to be affected by the roll directions.

When comparing the rolling moment results shown in Fig. 6 to the PIV measurements in Figs. 8 and 9, the triangular symbol at $\phi = 20$ deg when $\theta = 20$ deg in Fig. 6 corresponds to the PIV results in Fig. 8b and the rectangular symbol at $\phi = 20$ deg corresponds to the PIV results in Fig. 9b. The inboard vortex on the leeward wing when rolled in the counterclockwise direction has a higher absolute value of vorticity than that when rolled in the clockwise direction, as was seen in Figs. 8b and 9b. Therefore, in this case, the rolling moment stability has decreased. The absolute value of C_{roll} is smaller than that for the clockwise direction, as shown by the rectangular symbol at $\phi = 20$ deg in Fig. 6.

As noted in the Experimental Conditions section, the present measurements were obtained by stopping at each prescribed roll angle for about 3.5 sec, while rolling moment and PIV measurements were made. To make sure that the hysteresis was not affected by the resting time at each roll angle, additional rolling moment measurements were made by doubling this resting time at each roll angle. The resulting measured C_{roll} still indicated rolling moment hysteresis very similar to the ones shown in Fig. 6.

Figure 10 shows the velocity distributions inside the inboard vortex at $x = 0.83c_r$ for $\theta = 20$ deg and $\phi = 18$, 20, 22 and 24 deg, when rolled either in the clockwise or counterclockwise direction. The velocity distributions w_b along the line parallel to the y_b axis are indicated (the explanatory sketch in the figure). This line includes the vortex center position for the inboard vortex on the leeward wing. The center of the vortex location was determined from the measured velocity distributions by PIV when v_0 and $w_b = 0$ (v_b is the velocity component parallel to the y_b axis). Figure 10 shows that the velocity distributions w_b when rolled in the clockwise direction are relatively similar to those in the counterclockwise direction at $\phi = 18$ deg. The same tendency is seen at $\phi = 24$ deg. However, at $\phi = 20$ and 22 deg, absolute values of w_b when rolled in the counterclockwise direction are much higher than those when rolled in the clockwise direction. This is a signature of the velocity gradient existing at the center of the vortex, which is a typical feature of the leading-edge separation vortex just before breakdown [17], whereas the decrease in velocity gradient near the core region is a result of the vortex breakdown [18]. Therefore, the observed velocity difference between a clockwise and counterclockwise rotation at $\phi = 20$ and 22 deg indicates whether the vortex

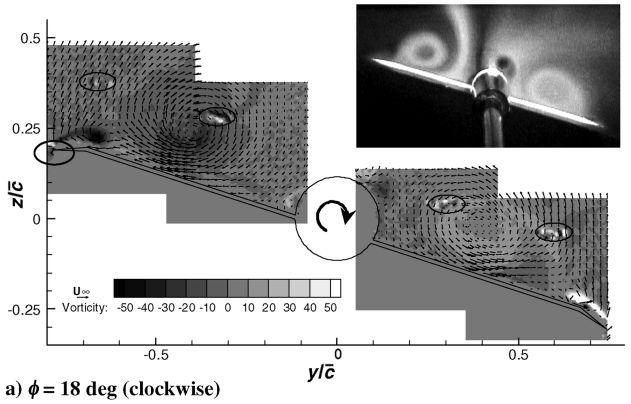

a) $\phi = 18$ deg (clockwise)

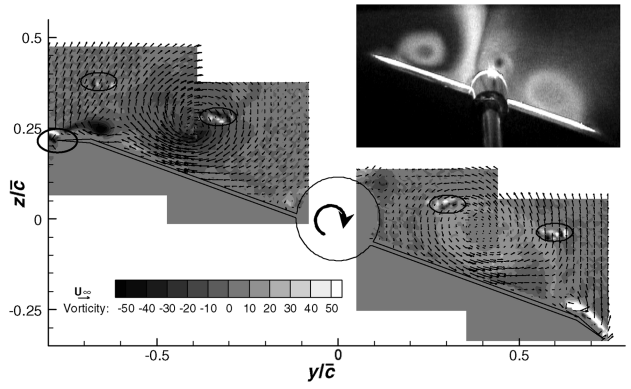

b) $\phi = 20$ deg (clockwise)

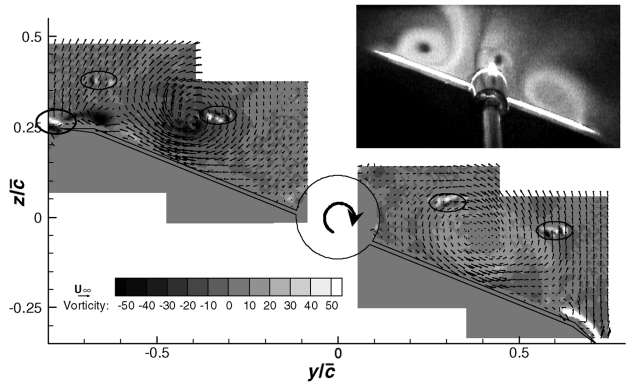

c) $\phi = 22$ deg (clockwise)

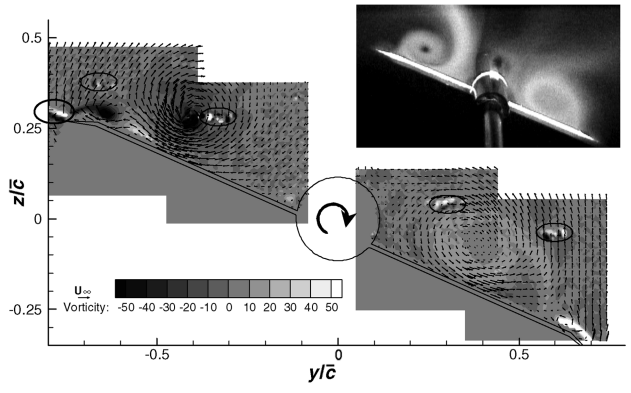

d) $\phi = 24$ deg (clockwise)

Fig. 8 Rolling moment characteristics at $\phi = 18$–24 deg, when the model is rolled in the clockwise direction from $\phi = -30$ to $+30$ deg at $\theta = 20$ deg, $x/c_r = 0.83$, S12 (with outboard flap deflection $\delta_{\mathrm{fLE}} = 12$ deg).

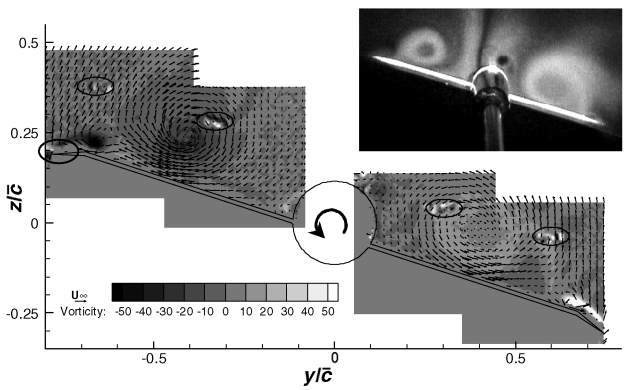

a) $\phi = 18$ deg (counterclockwise)

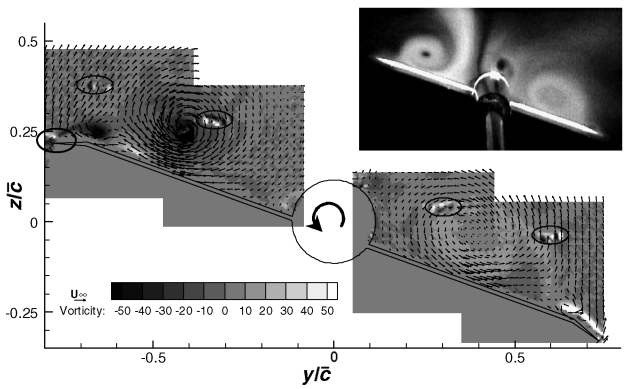

b) $\phi = 20$ deg (counterclockwise)

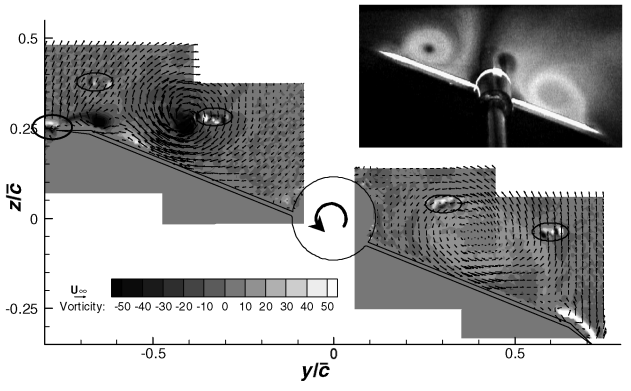

c) $\phi = 22$ deg (counterclockwise)

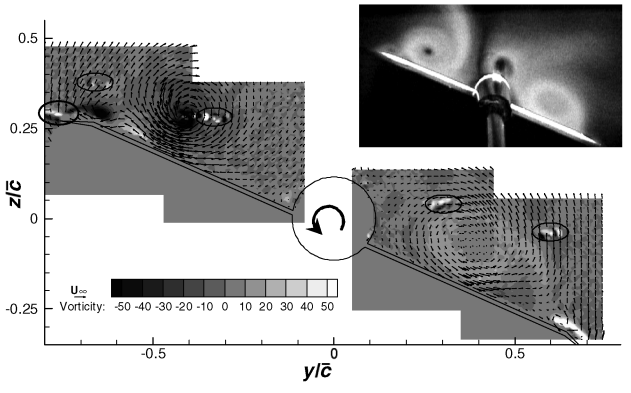

d) $\phi = 24$ deg (counterclockwise)

Fig. 9 Rolling moment characteristics at $\phi = 18$–24 deg, when the model is rolled in the counterclockwise direction from $\phi = +30$ to -30 deg at $\theta = 20$ deg, $x/c_r = 0.83$, S12 (with outboard flap deflection $\delta_{\mathrm{fLE}} = 12$ deg).

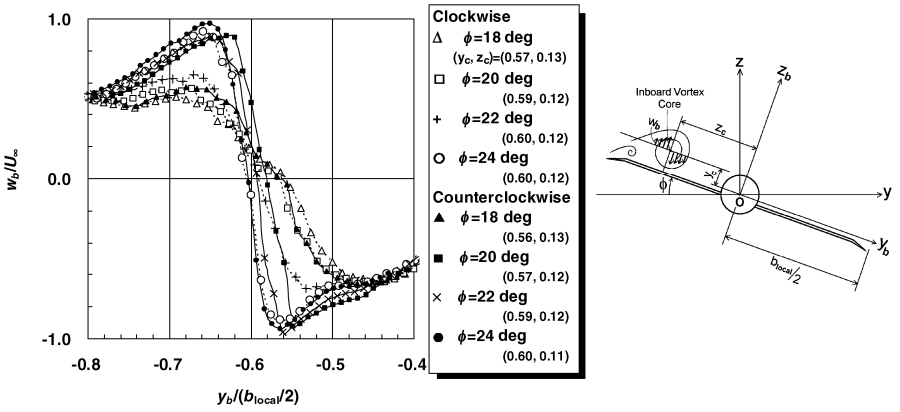

Fig. 10 The z_b-component velocity w_b distributions along the parallel line to the wing surface that include the inboard vortex center on the leeward wing of S12 (with outboard flap deflection $\delta_{\mathrm{fLE}} = 12\,\mathrm{deg}$, $\theta = 20\,\mathrm{deg}$, $x/c_r = 0.83$. b_{local} is the span length at $x/c_r = 0.83$ without flap deflection.

has broken down (lower velocity gradient of w_b) or not (higher velocity gradient of w_b). These results confirm the observations discussed in Figs. 8 and 9.

2. *Discussion on Rolling Moment Hysteresis*

Figure 11 shows the observed chordwise breakdown position for the inboard vortex on the left wing when $U_\infty = 10$ m/s. Results for S12 at $\theta = 16$, 20, and 26 deg are shown in Fig. 11a. Results for S00 at $\theta = 20$ and 26 deg and those for S12 at $\theta = 20$ deg are also shown in Fig. 11b. The breakdown positions were determined with the aid of smoke flow visualization by observing the light sheet normal to the x axis located at different chordwise positions. Since the vortex breakdown position is not steady and exhibits fluctuations along the axis of the vortices [19], positions where the smoke-free region near the vortex core is clearly visible (closed symbol) and where this region is not visible at all (open symbol) are indicated in this figure. It is thought that the breakdown occurs between these positions.

Figures 11a and 11b indicate that the breakdown position on the windward wing (left wing, $\phi < 0$) is relatively insensitive to the roll angle. On the leeward wing of S12 at $\theta = 20$ deg shown in Fig. 11a, the breakdown position rapidly moves from $x/c_r \approx 0.85$ to the trailing edge at $\phi \approx 20$ deg. This rapid movement of the breakdown position near the trailing edge was also observed on delta wings that have different sweepback angles [20]. Figure 6 indicated that there is rolling moment hysteresis at this roll angle. Jobe et al. [15] discussed that this hysteresis is caused by the vortex breakdown rapidly crossing the trailing edge. This agrees with the observations for S12 in Fig. 11a. It must be noted that the hysteresis of flow pattern is not recorded in this figure, because Fig. 11 was obtained by fixing the model independently at each roll angle to observe the breakdown position. Figure 11a also indicates the breakdown position of S12 for $\theta = 16$ and 26 deg when the rolling moment hysteresis was not observed. Although the breakdown is observed near the trailing edge when $\theta = 16$ deg, no rapid movement of the breakdown position is observed within the measured roll angles for $\theta = 16$ and 26 deg. This also supports the results as in [15] that the rolling moment hysteresis is caused by the rapid movement of the breakdown position at the trailing edge.

Figure 11b shows that the distributions of breakdown position of S00 at $\theta = 20$ deg are similar to that of S12 at $\theta = 20$ deg but are located relatively downstream of S12 almost for the whole roll angle. Rapid movement of breakdown near the trailing edge is also observed for S00 at $\theta = 20$ deg near $\phi = 20$ deg and at $\theta = 26$ deg near $\phi = 30$ deg. However, the rolling moment hysteresis was not observed for these configurations in Fig. 3. A question arises why the rolling moment hysteresis was observed for S12 but not for S00. As described at the beginning of Sec. III.B, the PIV measurements in Fig. 4 (S00) and Fig. 7 (S12) indicated that the outboard vortices are located much closer to the inboard vortex for S00 than that for S12 at $\theta = 20$ deg when $\theta = 0$, 10, and 20 deg at $x/c_r = 0.83$. This means that the two vortices on S00 may be interacting much more strongly with each other when compared with those on S12. Brennenstuhl and Hummel [2] showed that the interaction between inboard and outboard vortices formed on the double delta wing affects the vortex breakdown characteristics. This suggests that the different interactions between the inboard and the outboard vortices for S00 and S12 may have affected the vortex breakdown position for these two configurations. Verhaagen, et al. [21] reported that the breakdown of the inboard vortex will be triggered by the burst of the outboard vortex for the 76/40 deg double delta wing. It is thought that the inboard and outboard vortices formed on S00 affected each other in a similar manner to those formed on the wing in [21]. This may appear to have offered a possibility to avoid the rolling moment hysteresis for S00. On the contrary, since two vortices on S12 behave independently, the rolling moment hysteresis observed was quite similar to those for delta wings [15,16].

3. *Some Comments on Other Issues*

Other rolling moment characteristics that should be specially mentioned in Fig. 6 are that at $\theta = 18$ and 20 deg the slope of the C_{roll} versus the ϕ curve is locally positive near $\phi = 0$ deg. This locally unstable C_{roll} slope at $\phi = 0$ deg was also observed on a 65 deg delta wing at higher than 30 deg incidence angle [22]. Ericsson [22] discussed how the movement of vortex breakdown will generate a statically unstable C_{roll} slope at $\phi = 0$ deg. However, as Fig. 11 indicates, the breakdown movement is very small near $\phi = 0$ deg. Further investigation would clarify this phenomenon.

As described earlier, the tested Reynolds number based on $\bar{c}$ was $Re = 6.2 \times 10^4$ for the present model. The tested Reynolds numbers for the original model in [7–9] were $Re = 9.2 \times 10^5$. The difference of the Reynolds number may have affected the present results as discussed at the end of section III. References [23,24] investigated the sensitivity of double delta wing performance to the Reynolds number. Although the effect of the Reynolds number on force measurements is small, the inboard and outboard vortices are coiled up at low Reynolds number but remain separated at high Reynolds number [24]. The reported critical Reynolds number based on the root chord in [24] was the order of 10^4 and it was dependent on the wing leading-edge sweepback angle. This suggests that both the flow around the present SST configuration and the rolling moment hysteresis observed in this paper may indicate different characteristics when tested at Reynolds numbers greater than 10^5. Further investigation is also needed to clarify the effects of Reynolds number on the SST static roll characteristics and rolling moment hysteresis effects.

This paper discussed the static roll characteristics of the SST configuration. As for dynamic roll characteristics, Ericsson [1] showed that wing rock occurs on sharp-edged delta wings with leading-edge sweeps exceeding 74 deg. There is a possibility in the present case that the flow over the upper surface from the center body will cause also a 66 deg inboard wing to experience slender wing

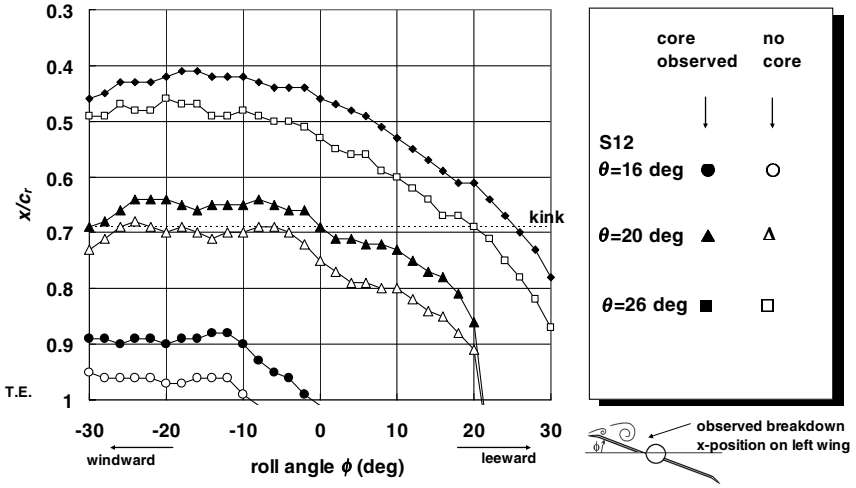

a) S12 (with outboard flap deflection $\delta_{fLE} = 12$ deg) at $\theta = 16$, 20, and 26 deg

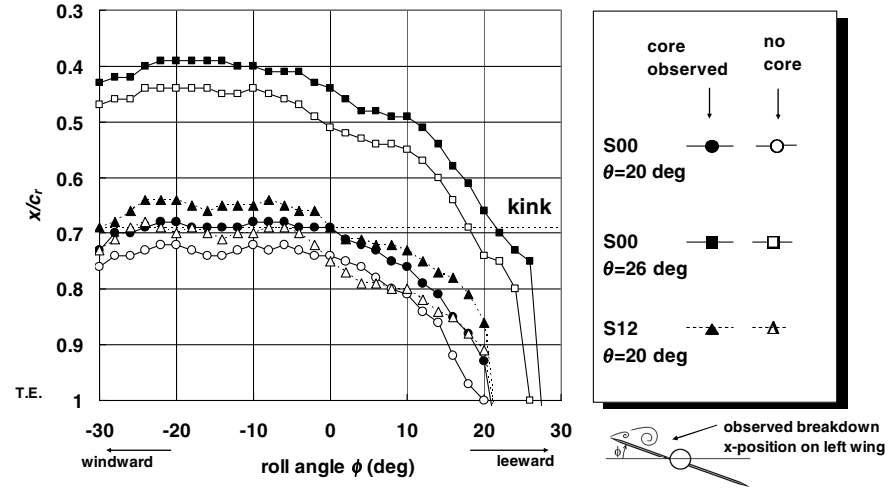

b) S00 (without flap deflection) at $\theta = 20$ and 26 deg, and S12 (with outboard flap deflection $\delta_{fLE} = 12$ deg) at $\theta = 20$ deg

Fig. 11 Effect of roll angle on vortex breakdown: observed breakdown x-positions on the left wing.

rock. However, it should also be pointed out that outboard 42 deg swept wing with its sharp leading edges will at high angles of attack generate sufficient damping to prevent wing rock from occurring for this configuration.

IV. Conclusions

Wind tunnel measurements were made of a cranked arrow wing SST configuration with and without outboard leading-edge flaps. The purpose of the measurements was to investigate the effect of outboard leading-edge flap deflections on the static roll characteristics of the cranked arrow SST configuration at a Reynolds number based on the wing mean aerodynamic chord of 6.2×10^4.

1) Static rolling moment measurements confirmed linear restoring moment for the roll direction at incidence angles lower than about 16 deg for the models both with and without flap deflection. As the incidence angle increases, this linearity is lost and the rolling moment becomes statically unstable for both configurations.

2) When the outboard leading-edge flap is deflected 12 deg, rolling moment hysteresis is observed at the roll angle $\phi \approx 20$ deg and incidence angle $\theta \approx 20$ deg. Crossflow velocity measurements at 83% chordwise position revealed that the vortex formed on the inboard wing does break down at a lower roll angle when the model is rolled in the clockwise direction (seen from downstream) than when the model is rolled in the counterclockwise direction. It was indicated that chordwise position of the vortex breakdown on the inboard wing is different when the wing is rotated in the clockwise and counterclockwise directions. This difference of vortex breakdown position caused the observed rolling moment hysteresis.

Acknowledgment

The authors gratefully acknowledge Yasuto Sunada of University of Tokyo for his helpful support of wind tunnel measurements.

References

[1] Ericsson, L. E., "The Fluid Mechanics of Slender Wing Rock," *Journal of Aircraft*, Vol. 21, No. 5, 1984, pp. 322–328.

[2] Brennenstuhl, U., and Hummel, D., "Vortex Formation over Double-Delta Wings," International Council of the Aeronautical Sciences Paper 82-6.6.3, Aug. 1982, pp. 1302–1309.

[3] Orsen, P. E., and Nelson, R. C., "Vortex Interaction Over Double Delta Wings at High Angles of Attack," AIAA Paper 89-2191, Jul. 1989.

[4] Hanff, E. S., and Jenkins, S. B., "Large-Amplitude High-Rate Roll Experiments on a Delta and Double Delta Wing," AIAA Paper 90-0224, Jan. 1990.

[5] Rao, D. M., "Leading Edge Vortex-Flap Experiments on a 74 Deg. Delta Wing," NASA CR-159161, Nov. 1979.

[6] Rinoie, K., and Stollery, J. L., "Experimental Studies of Vortex Flaps and Vortex Plates," *Journal of Aircraft*, Vol. 31, No. 2, 1994, pp. 322–329.
[7] Rinoie, K., Miyata, K., Kwak, D. Y., and Noguchi, M., "Studies on Vortex Flaps with Rounded Leading Edges for Supersonic Transport Configuration," *Journal of Aircraft* , Vol. 41, No. 4, 2004, pp. 829–838.
[8] Kwak, D.Y., Miyata, K., Noguchi, M., Rinoie, K., and Fujita, T., "Roll Characteristics of the SST Configuration with LE Flap and TE Flap at High Angles of Attack," AIAA Paper 2003-3413, Jun. 2003.
[9] Kwak, D.Y., Noguchi, M., Shirotake, M., and Rinoie, K., "Rolling Moment Characteristics of Supersonic Transport Configuration at High Incidence Angles," *Journal of Aircraft* (to be published).
[10] Sakata, K., "Supersonic Experimental Airplane (NEXST) for Next Generation SST Technology—Development and Flight Test Plan for the Unmanned Scaled Supersonic Glider," AIAA Paper 2002-0527, Jan. 2002.
[11] Anon., *DANTEC FlowMap Installation & User's Guide*, Dantec Measurement Technology, Skovlunde, Denmark, 1997, pp 4.68–4.102.
[12] Anon., *PIV Handbook*, edited by Visualization Society of Japan, Morikita Shuppan, Tokyo, 2002, pp. 137–164 (in Japanese).
[13] Arena, A. S., and Nelson, R. C., "Unsteady Surface Pressure Measurements on a Slender Delta Wing Undergoing Limit Cycle Wing Rock," AIAA Paper 91-0434, Jan. 1991.
[14] Grismer, D., Nelson, R., and Ely, W., "The Aerodynamic Effects of Sideslip on Double Delta Wings," AIAA Paper 93-0053, Jan. 1993.
[15] Jobe, C. E., Hsia, A. H., Jenkins, J. E., and Addington, A., "Critical States and Flow Structure on a 65-Deg Delta Wing," *Journal of Aircraft*, Vol. 33, No. 2, 1996, pp. 347–352.
[16] Katz, J., and Levin, D., "Static Measurements of Slender Delta Wing Rolling Moment Hysteresis," *Journal of Aircraft*, Vol. 28, No. 4, 1991, pp. 282–283.
[17] Earnshaw, P. B., "An Experimental Investigation of the Structure of a Leading-Edge Vortex", Aeronautical Research Council (ARC) Reports and Memoranda 3281, London, Mar. 1961.
[18] Visser, K. D., Iwanski, K. P., Nelson, R. C., and Ng, T. T., "Control of Leading Edge Vortex Breakdown by Blowing," AIAA Paper 88-0504, Jan. 1988.
[19] Gursul, I., and Yang, H., "On Fluctuations of Vortex Breakdown Location," *Physics of Fluids*, Vol. 7, No. 1, 1995, pp. 229–231.
[20] Wentz, W. H., and Kohlman, D. L., "Vortex Breakdown on Slender Sharp-Edged Wings," *Journal of Aircraft*, Vol. 8, No. 3, 1971, pp. 156–161.
[21] Verhaagen, N. G., Jenkins, L. N., Kern, S. B., and Washburn, A. E., "A Study of the Vortex Flow over a 76/40-deg Double-Delta Wing," AIAA Paper 95-0650, Jan. 1995.
[22] Ericsson, L. E., "Effect of Angle of Attack on Roll Characteristics of 65-Degree Delta Wing," *Journal of Aircraft*, Vol. 34, No. 4, 1997, pp. 573–575.
[23] Hebbar, S. K., Platzer, M. F., and Fritzelas, A. E., "Reynolds Number Effects on the Vortical Flow Structure Generated by a Double-Delta Wing," *Experiments in Fluids*, Vol. 28, No. 3, 2000, pp. 206–216.
[24] Gursul, I., Taylor, G., and Wooding, C. L., "Vortex Flows over Fixed-Wing Micro Air Vehicles," AIAA Paper 2002-0698, Jan. 2002.